Free-space optical communications link at 1550 nm using multiple-quantum-well modulating retroreflectors in a marine environment

W. S. Rabinovich
R. Mahon
H. R. Burris, MEMBER SPIE
G. C. Gilbreath
P. G. Goetz
C. I. Moore, MEMBER SPIE
M. F. Stell
M. J. Vilcheck
J. L. Witkowsky
L. Swingen
M. R. Suite
E. Oh, MEMBER SPIE
J. Koplow
U. S. Naval Research Laboratory
Washington, D.C. 20375
E-mail: Rabinovich@nrl.navy.mil

Abstract. A 1550-nm eye-safe, free-space optical communications link is demonstrated at rates up to 5 Mbits/s over a distance of 2 km in the Chesapeake Bay, using quantum-well-based modulating retroreflectors. Tests are conducted under various atmospheric conditions over a time period of about a year. The experimental and theoretical link budgets are compared and statistical measurements of the effects of scintillation are collected.
[DOI: 10.1117/1.1906230]

Subject terms: optical communications; quantum-well devices; retroreflector.

Paper 040409 received Jun. 23, 2004; revised manuscript received Nov. 4, 2004; accepted for publication Nov. 24, 2004; published online May 4, 2005.

1 Introduction

Free-space optical links (lasercomm) are finding increasing use for commercial systems and are being considered for military systems.[1–4] The narrow divergence and high bandwidth of optical beams enable point-to-point data links at rates exceeding 1 Gbits/s. However, these links require large telescopes, lasers, and highly accurate pointing systems to work. There are many situations in which one end of the link cannot accommodate the weight of a lasercomm terminal. These asymmetric links often have lower data requirements than a conventional lasercomm link because the smaller platform may have the capacity for only a moderate (1 to 100 Mbits/s) data rate sensor. An optical link may still be desirable in these cases because rf terminals for these data rates would be large, rf spectrum allocation may be limited, and because optical links are difficult to intercept. For this class of problems, a modulating retroreflector (MRR) link is appropriate.

An MRR couples a passive optical retroreflector such as a corner-cube or cat's eye with an electro-optic modulator. Figure 1 shows a diagram of a corner-cube-based MRR. In an MRR link, a conventional, actively pointed, lasercomm terminal on one end interrogates an MRR on the other end of the link with a continuous wave laser beam. This beam is passively retroreflected back to the interrogator with a signal imposed on it by the modulator.

MRRs were used in the past, but have typically been limited in their data rate by the choice of the electro-optic modulator. A link at a range of over 30 km was demonstrated using[5] a liquid crystal MRR. However, its data rate was limited to 10 kbits/s by the switching time of the liquid crystal. An MRR system using coherent CO_2 transmission was also demonstrated[6] but with a bandwidth of just 3 kbits/s. In addition, passive retroreflector links have been used to characterize the atmosphere,[7] to fold conventional lasercomm links,[8] and for satellite laser ranging.[9]

For the past 7 yr the Naval Research Laboratory (NRL) has worked on the development of MRR systems based on multiple-quantum-well (MQW) modulators.[10,11] MQW modulators are semiconductor p-i-n devices whose inherent switching rate exceeds 1 GHz. In practice, with MRR links, this switching rate is limited by the resistance-capacitance (RC) time constant of the device. We investigated two forms of MQW MRR. One is based on corner-cube retroreflectors and is capable of data rates up to about 10 Mbits/s using 0.63-cm-diam retroreflectors.[12] The other, based on cat's-eye retroreflectors, is capable of rates up to hundreds of megabits per second[13,14] and was demonstrated by us at rates up to 70 Mbits/s with a 1.6-cm aperture.[15]

In the past, we demonstrated MRR links at a wavelength of 980 nm to a small unmanned aerial vehicle (UAV) using this technology.[16] Those links were over a range of a few hundred feet, limited by the necessity of using broad divergence laser beams for laser eye-safety considerations. To address this issue we have developed MQW MRR that work at 1550 nm, an eye-safe wavelength.

Here we report on a 5-Mbits/s MQW MRR link at 1550 nm over ranges of up to 2 km. The link was from an interrogator on the shore to a boat on Chesapeake Bay. We describe the design of the MRR array and its relevant figures of merit. In addition, analysis of the link data provides insight into the effects of atmospheric turbulence on the optical link, as investigated through probability distribution functions and power spectral density profiles, and, in turn, the derived fade rate plots show the feasibility of using such free-space links in a maritime environment.

2 MQW MRRs

The operation of corner cube MRRs is determined primarily by the characteristics of the modulator that they use. MQW modulators are based on III-V semiconductors grown epitaxially on a substrate.[17] The MQW consists of alternating very thin layers of at least two materials: a well

0091-3286/2005/$22.00

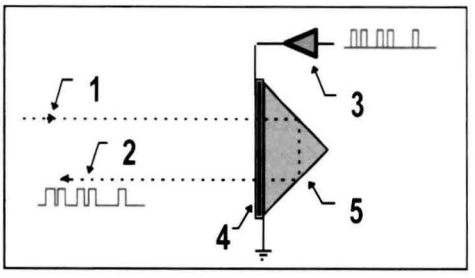

Fig. 1 Diagram of an MRR: 1, incoming beam; 2, outgoing, modulated beam; 3, data source; 4, multiple-quantum-well modulator; 5, corner-cube retroreflector.

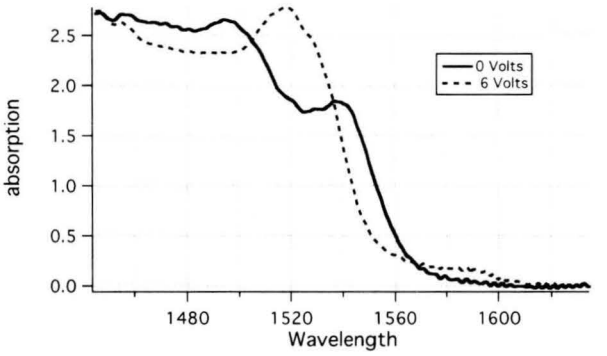

Fig. 2 Optical absorption of the coupled quantum well at two different bias voltages: 0 and 6 V.

and a barrier. Typical layer thicknesses are less than 10 nm and total active region thicknesses are a few micrometers. MQW modulators work by changing their optical absorption when a voltage is applied. The absorption change takes place over a range of wavelengths near the band edge of the well material. The strength of the absorption change and the voltage required to achieve it are determined by the layer structure of the MQW.

Optically, the most important characteristic of an MQW modulator is its contrast ratio, which is simply the ratio of its transmission in its "on" state divided by the transmission in its "off" state. MQW modulators are often used in waveguide mode. But for an MRR application, they must be used in surface-normal mode. This limits the contrast ratio that is achievable because the optical interaction length can only be twice the device thickness. Typical contrast ratios are between 2:1 and 3:1.

Electrically, MQW modulators take the form of a large area p-i-n diode. The intrinsic switching time of an MQW modulator is limited by its RC time up to data rates of gigahertz, where R is the electrical resistance and C the capacitance. This RC time is determined by the device capacitance, which is related to the required optical aperture, and the sheet resistance, which is determined by the electrode design. The design of an MRR link must balance using a large optical aperture, to return sufficient light, and the RC time of the device.

For the links reported here, we used an MRR with a 0.63-cm-diam aperture. The MQW MRR is based,[11] on InGaAs/InAlAs quantum wells grown on InP. The MQW was surrounded by a p-type InAlAs electrode on top and an n-type InAlAs electrode on the bottom. These devices operate around 1.55 μm, which is desirable from an eye-safety point of view. Two different kinds of MQW layer structures were used. For the first set of links we used a simple square well, which required a drive voltage of 10 to 15 V, and for the second set of links we used a more sophisticated coupled-well structure,[18,19] which required 4 to 6 V. For both structures, higher drive voltages produced higher contrast ratios. The coupled-well structure consumed approximately eight times less power at the same data rate as the square well, because the MQW power consumption scales as CV^2, where V is the drive voltage. Both structures produced contrast ratios of more than 2:1 when operated at their peak wavelength. Figure 2 shows the optical absorption of the coupled quantum well with and without bias.

In considering the optimal MQW structure to use for an MRR link, it is important to consider both the modulator and the nature of the optical receiver used on the interrogator terminal. At data rates of a few megabits per second, typical optical telecommunication detectors such as erbium-preamplified photodiodes do not work effectively due to the lack of extremely narrowband optical filters for limiting spontaneous emission noise. Instead InGaAs p-i-n diodes or avalanche photodiodes are used. As a result, the noise in the optical receiver is generally dominated by the noise of the electronic preamplifier circuit. Unlike quantum-limited systems, in which the noise level increases as the optical contrast ratio decreases, the noise level in this case depends only on the strength of the ac-coupled signal. The optical signal-to-noise ratio (OSNR) can then be defined as

$$\mathrm{OSNR}=\frac{P_{\mathrm{on}}-P_{\mathrm{off}}}{P_{\mathrm{noise}}}=P_{\mathrm{ret}}\frac{\exp(-\alpha_{\mathrm{on}})-\exp(-\alpha_{\mathrm{off}})}{P_{\mathrm{noise}}}, \qquad (1)$$

where P_{on} is the optical power returned by the MQW MRR when it is in its high transmission state, P_{off} is the power returned in the low transmission state, P_{noise} is the noise-equivalent power of the detector, P_{ret} is the optical power returned by the MRR excluding losses in the MQW modulator, and α_{on} is the double-pass absorption-length product of the MQW in its high transmission state and α_{off} in its low transmission state. From Eq. (1) we can see that maximizing the OSNR depends on both the optical contrast ratio and the optical transmission of the MQW. This can be seen more clearly by defining a figure of merit for the MQW, its modulation efficiency:

$$M=\exp(-\alpha_{\mathrm{on}})-\exp(-\alpha_{\mathrm{off}})=\exp(-\alpha_{\mathrm{off}})(C_{\mathrm{MQW}}-1), \qquad (2)$$

where M is the modulation efficiency, and C_{MQW} is the optical contrast ratio of the MQW. The OSNR of an MQW MRR link is then simply $MP_{\mathrm{ret}}/P_{\mathrm{noise}}$. This figure of merit makes it clear that increasing the MQW contrast ratio by increasing its thickness does not always improve link performance. This is because the increased contrast ratio will come at the cost of reduced optical transmission.

The contrast ratio and modulation efficiency of the coupled-well MQW is shown in Fig. 3. While the contrast

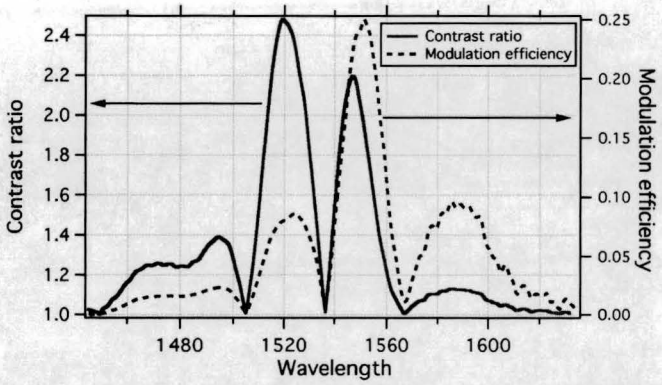

Fig. 3 Contrast ratio and modulation efficiency of a coupled-well MQW as a function of wavelength when modulated using a 0 to 6-V drive pulse.

ratio is highest near 1520 nm, the OSNR will be highest at the longer wavelength peak near 1550 nm. In addition, the very low contrast ratio peak near 1570 nm produces a relatively high modulation efficiency due to the higher optical transmission in the longer wavelength wing of the MQW absorption feature.

While the modulation efficiency determines the OSNR, other issues must be considered. If the received signal is dc coupled, the signal will consist of a small modulation riding on a slowly, but strongly, varying level due to atmospheric scintillation. As we show later, the time scale of scintillation is three or more orders of magnitude slower than the data rate, so these atmospheric variations do not show up as noise on the time scale of an individual bit. However, they can reduce the overall signal level below the sensitivity of the detector, and they slowly shift the threshold that distinguishes a 1 from a 0 in a digital signal. The first effect is similar to what happens in all free-space optical links and can be dealt with by adding margin or smart retransmission protocols to the link. The second effect can be dealt with using an adaptive threshold or even more simply by ac coupling of the signal. However, the signal processing for a very low contrast modulator, even if it has high optical throughput, will be more difficult than a higher contrast modulator. In practice, we have found an optical contrast ratio of between 1.5:1 to 2:1 to be sufficient for most links.

As we discuss in Sec. 5, the amount of light returned by a retroreflector depends strongly on its aperture. Since the MQW modulator must cover the aperture of the corner cube, very large area modulators are necessary. The modulators used in this experiment had a diameter of 0.65 cm and a capacitance of 2 to 3 nF. Because of the large capacitance of the devices and the high sheet resistance of the *p*-doped electrode layer, a webbed metal contact structure (shown in Fig. 4) was used to reduce the effective resistance of the *p*-doped layer.[12] This contact structure improved the speed of the MQW modulator by more than an order of magnitude over a simple ring contact and enabled a top modulation rate of about 5 Mbits/s. When operated at this data rate each modulator consumed about 60 mW.

Since MQW modulators use III-V semiconductors as their constituent materials their band edge shifts with temperature. Because the optical absorption change occurs over a finite band of wavelengths this means that for a fixed

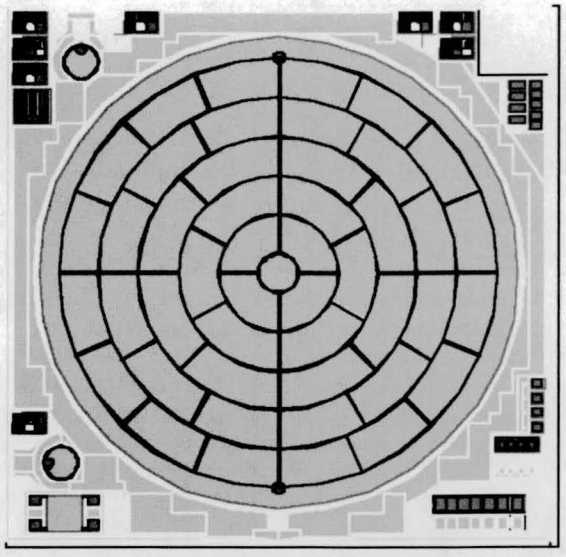

Fig. 4 Metal grid electrode pattern on the MQW modulator.

laser interrogator wavelength there is a fixed range of temperature over which the device returns a strong signal. For both the square-well and the coupled-well devices this temperature range was about 20°C. The center of this range is set by the interrogating laser wavelength. This enables a wavelength-agile interrogator to be used to extend the operational temperature range of the modulators. A tunable laser interrogator was used to set the interrogation wavelength to the peak response of the modulator. The 20°C operating range for a given interrogator wavelength is broad enough that it is generally sufficient to set a laser wavelength at the beginning of the day and leave it there. By tuning over the full bandwidth of an erbium fiber amplifier, temperature variations in excess of 80°C can be accommodated. It is also possible to stabilize the temperature of the modulator or alter its response in some other way to accommodate temperature drift, but these approaches increase the complexity of the system at the MRR end, which is generally not desirable.

3 Retroreflector Array Design

Corner-cube retroreflectors have a field of view (FOV) determined by their index of refraction and by whether their return is measured in the near field or in the far field. In the near field, the return drops with angle because the effective aperture of the corner cube is reduced when it is illuminated off normal incidence. In the far field, an additional reduction in intensity occurs due to the increased diffraction from this reduction in effective aperture. The reduction in the effective area of the corner cube can be described as[9]

$$\eta(\theta_{\text{inc}}) = \frac{2}{\pi}(\sin^{-1}\mu - \sqrt{2}\mu\tan\theta_{\text{ref}})\cos\theta_{\text{inc}}, \tag{3}$$

where θ_{inc} is the incident angle, θ_{ref} is the refracted angle in the corner cube, and μ is a quantity defined by

$$\mu = (1 - 2\tan^2\theta_{\text{ref}})^{1/2}. \tag{4}$$

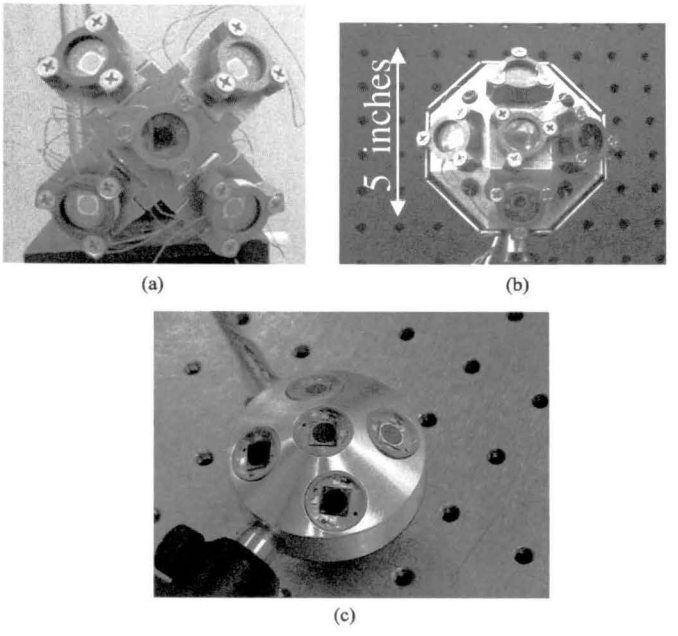

Fig. 5 Progression of array mounted MRRs.

For near-field retroreflection, the optical return is reduced by $\eta(\theta)$ and for far-field retroreflection by $\eta^2(\theta)$. The full width at half maximum FOV for a glass corner cube is then about 42 deg in the near field and 26 deg in the far field.

To relax the pointing requirements on the retroreflector end of the link, an array of retroreflectors was typically used. Initially, five MRRs were arranged on an umbrella-type structure with variable relative angle so that all five could be either coplanar or held at relative angles of up to 45 deg. This unit is shown in Fig. 5 along with two further embodiments where the modulators are set at 30 deg relative to each other. The choice of relative angle of 30 deg provides a maximum full FOV angle of about 60 deg with the response maintaining a level of at least 50% of the single MRR at normal incidence, as shown in Fig. 6.

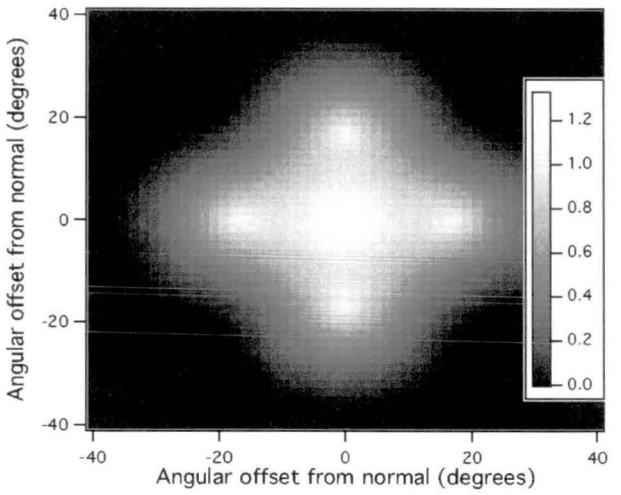

Fig. 6 Simulation of return from the array shown in Fig. 5(b). The gray scale indicates the strength of the return normalized to the return from a single retroreflector.

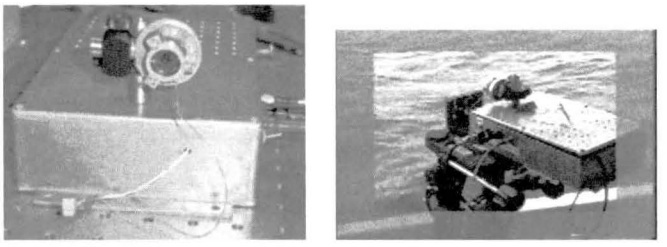

Fig. 7 Actual modulator unit in a digital camera picture taken in the lab (left) and in an image extracted from a still frame from the optically transmitted video at 1 km (right). The box contains the L3 wavelet compression unit and modulator drive electronics.

4 Field Experiments

The performance of the MQW MRR was tested by closing a free-space link to either a single device or to an array of devices mounted on a boat in the Chesapeake Bay. The interrogator was positioned on a cliff at an elevation of about 30 m and the range to the boat was varied from 0.5 to 2 km. This series of experiments was conducted under a variety of atmospheric conditions over the time period November 2002 to October 2003. There was no active pointing capability for the interrogator available for these tests. The transmitted signal was either derived from a pattern generator set to give a pseudorandom bit sequence (PRBS) or a square-wave modulation at rates of 250 kbits/s to 5 Mbits/s, or from a video compression unit set for 3 Mbits/s. Long-duration, high-resolution data sequences were recorded for up to 25 s at 20 megasamples/s and 7.5 s at 50 megasamples/s. Live video transmission was carried out during four of the tests. The long data sets were subsequently analyzed giving atmospheric information through the derived power spectral density dependences and the probability distribution functions.

Early experiments were done using the umbrella structure shown in Fig. 5(a) and the square-well MQW structure. Later experiments used the array shown in Fig. 5(b) with the coupled-well MQW modulators.

One of the objectives of this series of free-space communication tests was to assess the feasibility of transmitting real-time video signals in the presence of atmospheric turbulence. These experiments used a handheld Sony camcorder that produced a standard NTSC signal, which was digitized through an L3 wavelet compression system. This unit compressed a 15 frame/s video signal down to 3 Mbits/s. The digitized signal was then routed through an impedance-matching circuit to drive a single MRR at the 3-Mbits/s data rate. A photograph of the actual unit is shown in Fig. 7 together with a still frame extracted from a video transmitted by the unit itself.

An interrogator on the shore illuminated the MRR array. Since the ground station was on a cliff that was about 30 m above sea level, the optical path was pointed slightly downward to the water. The first interrogator consisted of a 1.5-W, 1550-nm NRL-designed erbium-doped fiber amplifier (EDFA), collimated to a full angle e^{-2} beam divergence of 1.3 mrad. The EDFA was seeded by a low-power laser, tunable from 1530 to 1580 nm to accommodate the variation of climatic temperature.

The interrogator was mounted on a gimbal but no closed-loop pointing was available. The outgoing laser

Table 1 The powers associated with all factors contributing to the link budget are shown, together with the general formulas used and the specific case of the 2 km range link conducted on October 29, 2003, are presented and show good agreement between predicted and actual received powers.

Term	Parameter	Formula	dB
Transmit power	4.2 W	Measured	36.2 dBm
Transmitter loss		Measured	−1.5
Transmitter antenna gain	Full angle e^{-2} divergence $\theta_{div}=0.83$ mrad	$\frac{32}{\theta_{div}^2}$ Gaussian beam underfilling transmit aperture	76.7
Range loss (interrogator)	Range, $R=2$ km $\lambda=1550$ nm	$\left(\frac{\lambda}{4\pi R}\right)^2$	−204.2
Atmospheric transmission	16-km visibility	Reported visibility	−0.6
MRR modulation efficiency, M	Coupled-well modulator	$\exp(-\alpha_{off})(C_{MQW}-1)$	−7.1
MRR loss	Loss due to antireflection	Measured	−0.7
MRR T/R antenna gain, G_{retro}	$D_{retro}=0.63$ cm	$\left(\frac{\pi D_{retro}}{\lambda}\right)^4$	164.3
Range loss (retroreturn)	Range, $R=2$ km $\lambda=1550$ nm	$\left(\frac{\lambda}{4\pi R}\right)^2$	−204.2
Atmospheric transmission	16-km visibility	Reported visibility	−0.6
Receiver antenna gain	$D_{rec}=7.5$ cm	$\left(\frac{\pi D_{rec}}{\lambda}\right)^2$	103.6
Receiver loss	Fiber coupling loss	Measured	−3
Predicted received power	70 nW		−41.1 dBm
Actual received power	44 nW		−43.5 dBm

beam was emitted through a 5-mm hole drilled at 45 deg in the center of a 4-in.-diam mirror and was aligned with the axis of the receive optics. The interrogator unit was mounted on a Meade tripod and manually pointed at the MRR array on the boat. The retroreflected beam carried the modulation imposed on it at the boat. The receive mirror then directed the return beam through an $f/2$ collection lens and a pair of coupling lenses into a 62.5/125-μm graded-index multimode fiber-connected p-i-n field-effect transistor (FET) photodetector with a 7-MHz bandwidth and −57-dBm sensitivity, a responsivity of 0.98 A/W, and a transimpedance amplifier stage giving an overall transfer gain of 1.08×10^6 V/W.

All data, with the exception of the October 29, 2003, data, were acquired using the 4-in. receive aperture system just described. However, the October test used a second interrogator that consisted of a 5-W Keopsys EDFA, the output of which was collimated to a full angle e^{-2} beam divergence of 0.8 mrad. A low-power laser, tunable from 1536 to 1560 nm, again seeded the EDFA. The interrogator was mounted on a Sagebrush gimbal with a 10-lb maximum weight limit that necessitated a miniaturization of the optics. The transmit laser beam was emitted through a 10-mm hole drilled at 45 deg in the center of a 4-in.-diam mirror and was aligned with the axis of the receive optics. The receive mirror directed the return beam through a 3-in.-diam limiting aperture $f/2$ collection lens and a pair of coupling lenses into a 100/140-μm graded-index multimode fiber-connected p-i-n FET photodetector with a 7-MHz bandwidth and −57-dBm sensitivity.

When the received signal contained an optically encoded video data stream, the output from the p-i-n FET was fed through a Femtovoltage electronic amplifier before being processed by a video expansion unit and bit-sync card, all from L-3 and housed in a laptop computer. In the lab, a receive signal level of 0.2 V was sufficient to regenerate the video but in the field an amplification of 20 to 30 dB provided by the electronic amplifier greatly improved the synchronization.

5 Link Budget

Careful measurements of conditions, and characterization of the interrogator's optical beam were undertaken to allow a comparison of the theoretical versus experimental link budget. Table 1 lists the factors involved in closing a two-way link to a single MRR unit of aperture D_{retro} at a range R, where the outgoing interrogating beam has a divergence angle of θ_{div} and the diameter of the limiting aperture of the receiver is D_{rec}. We define a retroreflector transmit/receive optical antenna gain G_{retro} for use in the link budget. This parameter is simply the product of the classical formulas for a diffraction-limited circular aperture used as a receiver and as a transmitter.[20] Other specific parameters, such as the actual laser powers and the visibility, are those pertinent to the tests conducted on October 29, 2003, when coupled-well modulators were used in an angled array. Experimentally, the link power varies due to both scintillation and pointing errors. Over a sufficiently long time (of the order of 1 s), the variations due to scintillation should average out

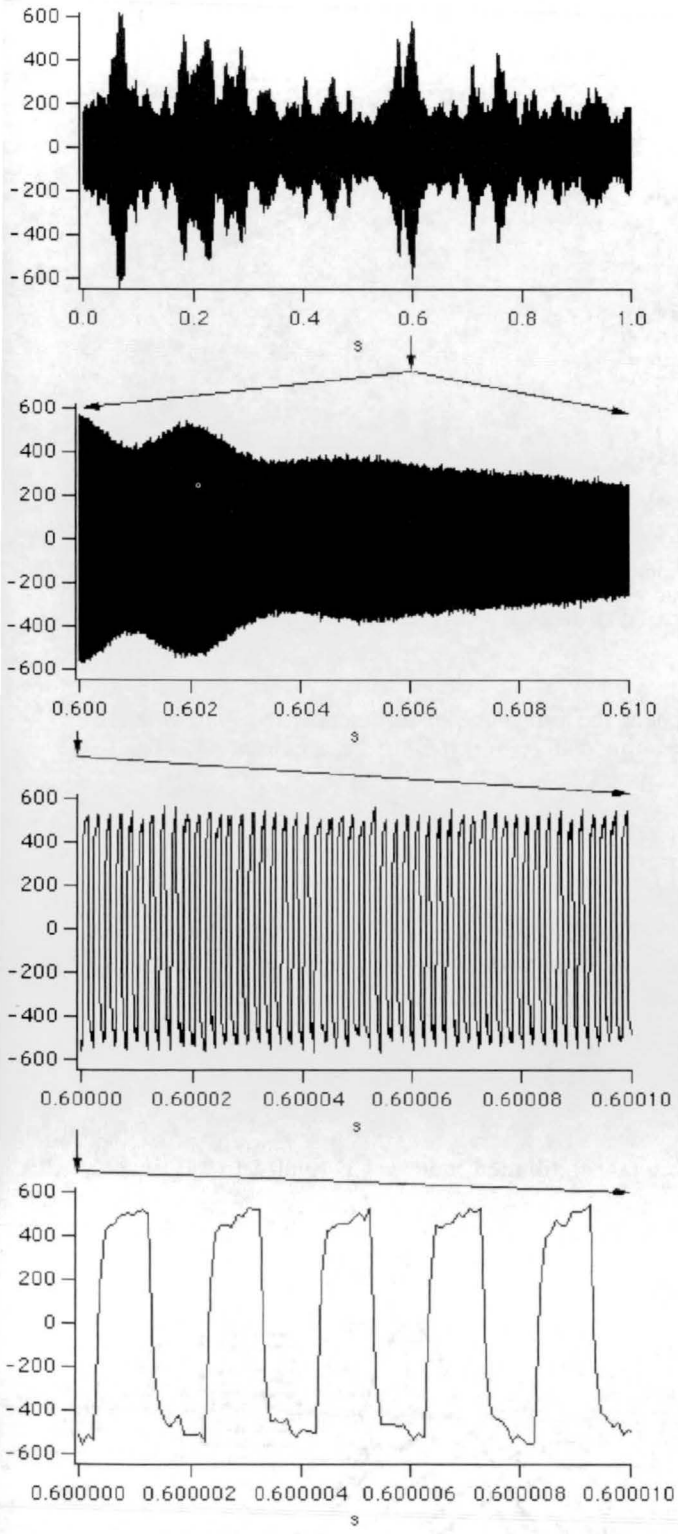

Fig. 8 Four time segments of data taken on October 29, 2003, showing the slow atmospheric variations and the imposed 1-Mbits/s square-wave modulation.

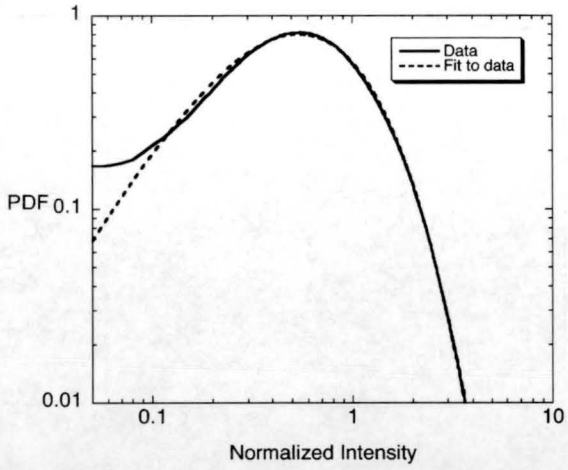

Fig. 9 PDF derived from the 7.5-s duration of data recorded on March 7, 2003, at a range of 2 km. The intensity was normalized to the mean intensity received. A PRBS at 250 kbits/s was returned from a 0.63-cm-diam MRR. The ΓΓ function best fit to the data is consistent with a Rytov parameter $\beta_0 = 0.72$ and a scintillation index $\sigma_I^2 = 0.312$.

to the mean value of the received power. In our link budget, we assume perfect pointing. However, the boat was in motion and no active tracking was used, so the interrogating beam was centered only on the MRR array for some of the time. To account for this we broke the 17-s-long data streams into 1-s-long segments and used the segment with the highest average for the experimental average in the link budget. Agreement between theory and experiment was very good, given the uncertainties in link parameters, with the actual received power lower by 2.4 dB than the expected power. This difference may be attributable to deviations in perfect diffraction limited return from the retroreflector.

6 Atmospheric Scintillation: Model

The long-length, high-sampling-rate data taken for the MRR links enabled a detailed comparison to theoretical treatments of the subject. We adopted the nomenclature and formulations developed by Andrews and Phillips.[21] In their model, the intensity fluctuations experienced by an optical

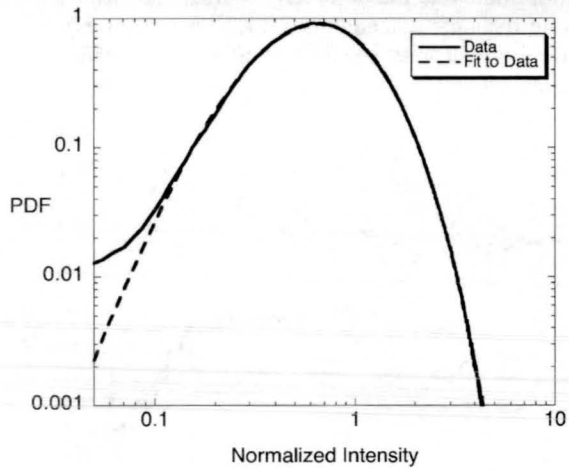

Fig. 10 PDF derived from the 7.5-s duration of data recorded on March 7, 2003, at a range of 1.6 km. The intensity was normalized to the mean intensity received. A PRBS at 250 kbits/s was returned from a 0.63-cm-diam MRR. The ΓΓ function best fit to the data is consistent with a Rytov parameter $\beta_0 = 0.57$ and a scintillation index $\sigma_I^2 = 0.236$.

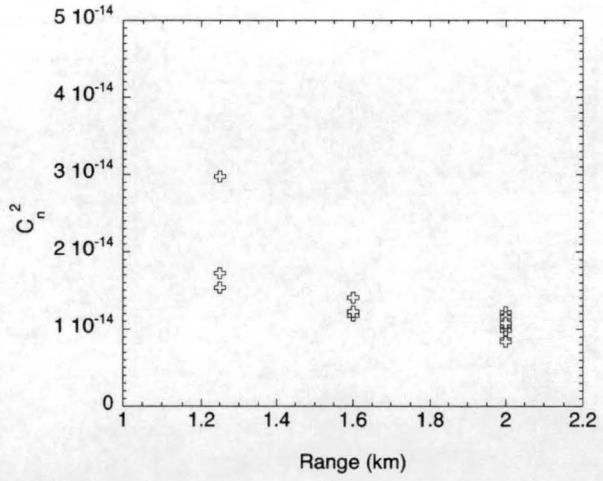

Fig. 11 Index of refraction structure parameter C_n^2 inferred from values of β_0 drawn from best fits of data to ΓΓ function versus one-way range. These data were recorded on March 7, 2003.

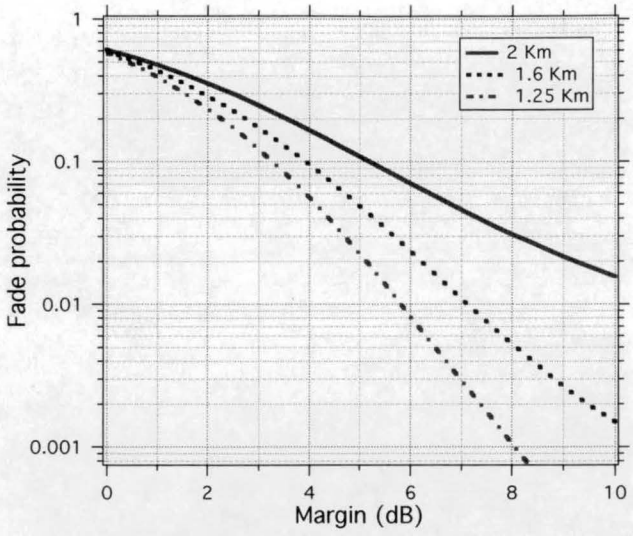

Fig. 13 Probability of a fade plotted as a function of margin, in decibels, of the received signal over detector sensitivity for data taken on March 7, 2003, at range values of 1.25, 1.6, and 2 km.

wave passing through the atmosphere are characterized by the scintillation index σ_I^2 which is a measure of the variance of the signal intensity:

$$\sigma_I^2 = \frac{\langle I^2 \rangle}{\langle I \rangle^2}. \tag{5}$$

In the limit of weak fluctuations and for the spherical wave model,

$$\sigma_I^2 = \beta_0^2 = 0.5 C_n^2 k^{7/6} L^{11/6}, \tag{6}$$

where β_0 is the Rytov variance, C_n^2 is the structure parameter for refractive index fluctuations, k is the wave number of the optical wave, and L is the range of propagation.

The probability distribution function (PDF) is generally accepted to follow a lognormal function when single scattering events dominate and the atmospheric fluctuations are weak. Increasing turbulence leads to multiple scattering effects and, in the limit of very strong turbulence, the irradiance statistics are expected to follow a negative exponential. To cover the full range of turbulence, the generalized gamma-gamma distribution (ΓΓ) of the irradiance has been proposed by Andrews et al.[22]

$$p(I) = \frac{2(\alpha\beta)^{(\alpha+\beta)/2}}{\Gamma(\alpha)\Gamma(\beta)} I^{(\alpha+\beta)/2-1} K_{\alpha-\beta}[2(\alpha\beta I)^{1/2}], \tag{7}$$

where $K_v(x)$ is a Bessel function of the second order, and α and β are directly related to the large-scale and small-scale scintillations σ_x^2 and σ_y^2 of the optical wave

$$\alpha = \frac{1}{\sigma_x^2} \quad \text{and} \quad \beta = \frac{1}{\sigma_y^2}, \tag{8}$$

while the total scintillation index σ_I^2 is related to these parameters by

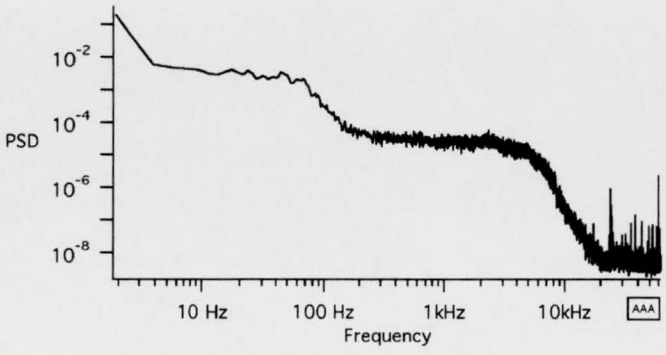

Fig. 12 PSD profiles derived from a 7.5-s-duration data stream consisting of on-off keying at 250 kbits/s applied to a modulator at a range of 1.62 km from the interrogator unit. These data were recorded on March 7, 2003.

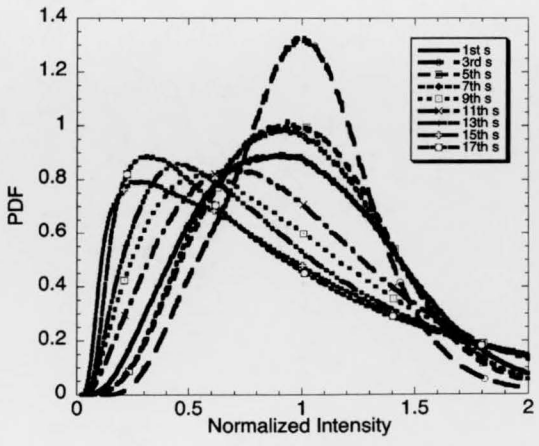

Fig. 14 PDFs measured over 1-s durations shown at 2-s intervals for a consecutive 17-s record of 1-Mbits/s modulated PRBS data returned from a MRR array located at a range of 1 km. The intensity was normalized to the mean intensity received.

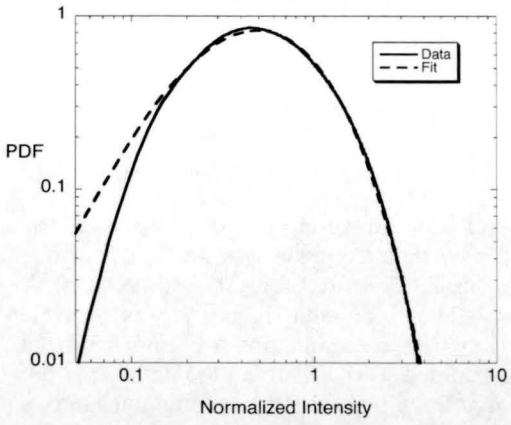

Fig. 15 PDF derived for a 1-s duration of data recorded on April 15, 2003, at a range of 1 km. The intensity was normalized to the mean intensity received. The data set corresponds to the 13th second of the data shown here. A PRBS at 1 Mbits/s was returned from a 6.3-mm-diam MRR. The ΓΓ function best fit to the data is consistent with a Rytov parameter $\beta_0 = 0.751$ and a scintillation index $\sigma_I^2 = 0.529$.

$$\sigma_I^2 = \frac{1}{\alpha} + \frac{1}{\beta} + \frac{1}{\alpha\beta}. \tag{9}$$

Note that σ_x^2 and σ_y^2 are evaluated in the spherical wave model both in the absence of inner-scale effects and in the presence of a finite inner scale, following the formulation in Ref. 22. Here the large-scale and small-scale variances are functions of the Rytov parameter β_0 and of the nondimensional parameter $Q_1 = 10.89L/kl_0^2$, where l_0 is the inner-scale length of the turbulence. Generally, l_0 is accepted to be in the range of 3 to 10 mm near the ground and takes lower values for higher turbulence conditions. However, when the actual data were fitted to the full inner-scale-dependence PDF, it was found that this formulation rarely provided any improvement to the fit over that found in the absence of including inner-scale effects. Indeed many values of l_0 fit the data equally well. Note also that there is

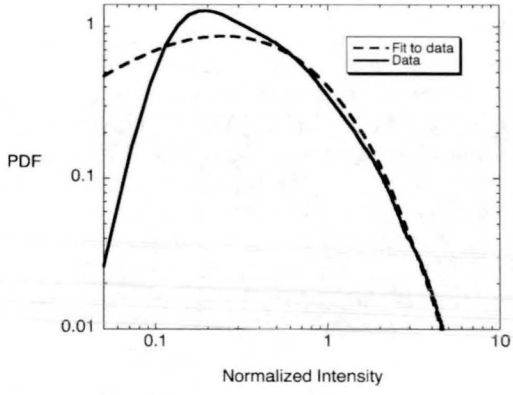

Fig. 16 PDF derived for a 1-s duration of data recorded on April 15, 2003, at a range of 1.6 km. The intensity was normalized to the mean intensity received. The data set corresponds to the 10th second of the 17-s-long data record. A PRBS at 1 Mbits/s was returned from a 0.63-cm-diam MRR. The ΓΓ function best fit to the data is poor, and the curve shown corresponds with a Rytov parameter $\beta_0 = 0.862$ and a scintillation index $\sigma_I^2 = 0.68$.

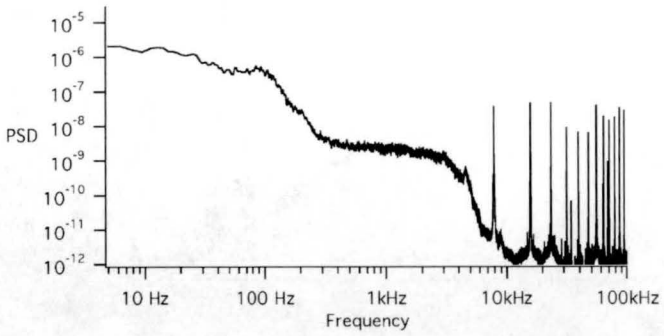

Fig. 17 PSD profiles derived from a 17-s-duration data stream consisting of a PRBS at 1 Mbits/s applied to a modulator at a range of 1.6 km from the interrogator unit. These data were taken during the April 15, 2003, test.

negligible difference in the scintillation index that results from the best fit to the PDF either including or excluding the inner-scale dependence, whereas there is a significant difference in the value of β_0. Thus, the data presented here are evaluated using the PDF for the spherical wave approach and with no inner-scale dependence. We also attempted using the simpler log-normal PDF function[22] and found that it gave substantially worse agreement with the data regardless of the parameters chosen.

Increased fluctuations above theoretical predictions would be expected if angle-of-arrival variations were sufficient to move the focal spot of the receive telescope off the multimode fiber that couples to the photodetector. In previous measurements over Chesapeake Bay, we found angle-of-arrival fluctuations to be about ± 50 μrad for a much longer optical path than that in this experiment.[8] Given the approximately 25 cm focal length of the receive optics, this corresponds to a spot wander in the focal plane of about 12 μm. This is much less than the 62- and 100-μm-diam multimode fibers used in the receivers, so we do not expect spot wander to be a problem.

We used the experimental data and Eq. (7) to characterize the scintillation in our links. A best fit of Eq. (7) to the

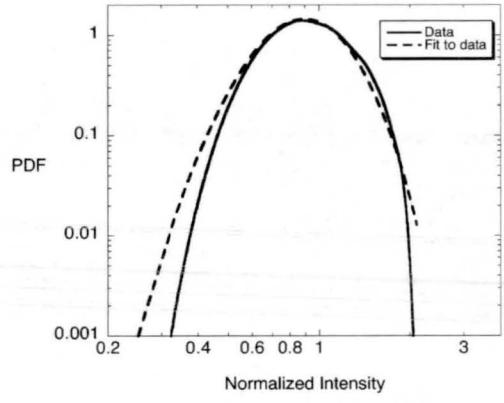

Fig. 18 PDF derived from a 25-s duration of data recorded on October 29, 2003, at a range of 1.6 km. A 1-Mbits/s data stream was returned from an angled array of five 0.63-cm-diameter MRRs. The ΓΓ function best fit to the data is consistent with a Rytov parameter $\beta_0 = 0.235$ and a scintillation index $\sigma_I^2 = 0.056$.

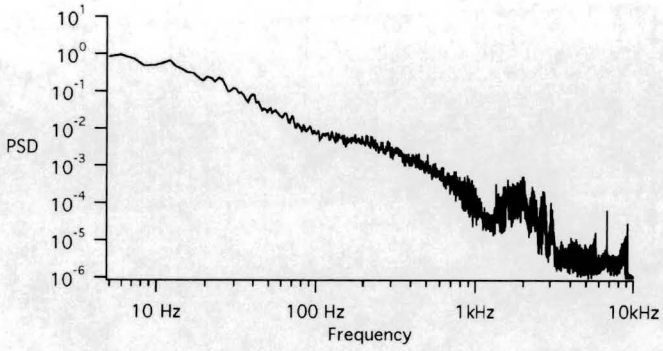

Fig. 19 PSD profiles derived from a 25-s-duration data stream at 1 Mbits/s applied to a modulator at a range of 1.6 km from the interrogator unit in the presence of light rain on October 29, 2003.

measured intensity fluctuations of a given data set infers an experimental determination of β_0 and, in turn, an implied value for the scintillation index σ_I^2.

In addition, since our measurements are taken over a monostatic return channel, where the modulator is effectively a point source and the receiver has a finite aperture, the resulting best-fit scintillation index must be scaled for a single path and a point receiver to be able to compare the fit parameters with independently measured values of the structure constant C_n^2. We use the single-to-double path relationship[22]

$$\sigma_I^2(2L) = \sigma_I^2(L)[4 + \sigma_I^2(L)], \tag{10}$$

and the aperture averaging factor A (Ref. 21):

$$A = \left[1 + 0.333\left(\frac{kD^2}{4L}\right)^{5/6}\right]^{-7/15}, \tag{11}$$

where D is the diameter of the receiver aperture.

The Rytov parameter β_0, which gives a scintillation index consistent with the single pass $\sigma_I^2(L)$, is then used to give a value of C_n^2 for the data set under consideration.

Theory[23,24] and experiment[25] predict an enhancement of both the backscattered intensity and the fluctuations of that intensity in a retroreflector link. The enhancement factor of both generally varies between 1.5 and 2 times. The width of the enhanced backscatter peak is approximately the first Fresnel zone. Since we have no spatial resolution in our receiver, we cannot verify the presence of this peak, however, the enhanced backscatter phenomenon is not likely to have a large effect on our experimental results. For our experimental conditions, this peak would have a width between 1.5 and 2.5 cm, depending on range. Since our receivers have either a 7.5- or 10-cm aperture, the effects of the enhanced backscatter will be diluted by a factor of 10 or more. In addition, since both our interrogators had 0.5- to 1-cm holes in the center of the receive optic to allow for the transmit beam, the strongest part of the enhanced backscatter peak never makes it into our receiver.

7 Data Analysis

Long-duration data sets of received signal intensities were acquired during three field tests conducted from the shore to a MRR array carried on a boat for ranges up to 2 km. The March 7, 2003, data used both a PRBS ($10^{23}-1$) and a square-wave modulating pulse profile at 250 kbits/s. The modulation rate was set by the digitizer used at that time, which enabled capture of only 2.5 megasamples/s for 7.5 s. Data taken after April 14, 2003, were acquired with a digitizer having an extended sampling rate of up to 50 megasamples/s and so modulation rates of up to 5 Mbits/s were then possible for data lengths of 7 s. At the lower rate of 1 Mbits/s, data could be stored for a 17-s time span.

For the square-wave-modulated signals, it was possible to measure the intensity as a function of time from the range of values recorded over a single modulation period. This was not possible with the PRBS modulation, and so these data had to be first adjusted for incomplete ac coupling by shifting the level by the slowly varying average of the signal and then taking the absolute value of the signal. Some relevant parameters associated with the double-pass link are given in Table 2 for ranges most commonly used in these tests.

For close-in ranges of 500 to 750 m, the return signal would often saturate the detector but the small beam size at the modulator made continuous pointing difficult for long-period acquisitions due to motion of the boat. For ranges of 2 km or more, the pointing from the interrogator was much easier, but the fourth-order fall-off with range for the returned signal made it necessary, for instance, to have all five MRRs contributing to the return signal when only 1.5 W of laser power was available and so, in that case, the pointing of the MRR from the boat became more critical.

An example of the raw data from a 7.5-s record is shown in Fig. 8 where four time segments are reproduced showing the typical atmospherically induced variations as well as the imposed higher frequency modulation. This plot demonstrates how the very different time scales of the data rate and the atmospheric fluctuations affect the signal. The scintillation fluctuations often exceed the 2:1 optical contrast ratio, but, since they do so on a slow timescale, the individual bits are never distorted. A summary of the data presented in this paper is given in Table 2.

The bandwidth (7 MHz) of the p-i-n FET detector was chosen to enable the imposed modulation (up to 5 Mbits/s) to be ac coupled while the highly variable dc component of the return signal below 20 kHz was effectively damped. Remaining variations due to incomplete ac coupling of the signal were dealt with by adjusting the level with a running average of the signal and then mapping the modulated signal strength with time. Histograms of the received intensity were derived from the data sets. The histograms were then normalized to an average intensity of 1 and the probability distribution was also normalized to an integrated value of 1. Sample normalized PDFs are shown in Figs. 9 and 10 for ranges of 2 and 1.6 km taken on March 7, 2003. Note that the OSNR of the link was generally 10 to 15 dB so that experimental data for intensities below about 10% of the mean are not reliable, being below the detector noise floor. This accounts, in part, for the deviation of the experimental and theoretical PDFs at low intensity.

Figure 11 shows the cumulative C_n^2 values deduced from the March 7 data and plotted as a function of the single-pass range parameter. Finally, Fig. 12 shows a typical power spectral density (PSD) plot, which was generated

Table 2 A summary is given of all the turbulence parameters deduced from the data taken on the three test dates described in this paper, namely, March 7, April 15, and October 29, 2003, as well as the pertinent weather related conditions as measured at Thomas Point buoy, a weather station near the test site. WndSpd is the wind speed in meters/second, WtrT is the water temperature in degrees C and AirT is the air temperature in degrees C.

Date	Range (km)	β_0	σ_I^2	$C_n^2(\times 10^{-14})$	Thomas Point Buoy	Air Temperature at Boat	Data Length (s)
3-7-03	2	0.72	0.312	1.083	a	1.6	7.5
		0.69	0.289	1.003	a	1.6	7.5
		0.636	0.250	0.863	a	1.6	7.5
		0.625	0.242	0.836	a	1.6	7.5
		0.683	0.284	0.985	a	1.6	7.5
		0.706	0.301	1.046	a	1.6	7.5
		0.763	0.345	1.215	a	1.6	7.5
		0.745	0.331	1.154	a	1.6	7.5
		0.718	0.311	1.079	a	1.6	7.5
	1.6	0.617	0.270	1.406	b	0.9	7.5
		0.561	0.226	1.173	b	0.9	7.5
		0.574	0.236	1.226	b	0.9	7.5
	1.25	0.469	0.189	1.535	c		7.5
		0.497	0.211	1.722	c		7.5
		0.66	0.359	2.974	c		7.5
04-15-03	1.6	1.1	0.683	3.879	d		17
	1.6	0.618	0.271	1.411	d		17
	1	0.335	0.114	1.395	e	14.7	17
10-29-03	1	0.342	0.101	1.236	f	13	25
	2	0.479	0.129	0.4436	g		25
	1.6*	0.294	0.056	0.288	h		25

[a]WndSpd, 5.8 m/s; WtrT, 0.7°C; AirT, −3.6°C.
[b]WndSpd, 6.5 m/s; WtrT, 0.8°C; AirT, −3.2°C.
[c]WndSpd, 6.8 m/s; WtrT, 0.9°C; AirT, −3.1°C.
[d]WndSpd, 7.5 m/s; WtrT, 9.3°C; AirT, 10.7°C.
[e]WndSpd, 7.3 m/s; WtrT, 9.5°C; AirT, 10.4°C.
[f]WndSpd, 6.8 m/s; WtrT, 15.2°C; AirT, 9.8°C.
[g]WndSpd, 4.9 m/s; WtrT, 15.2°C; AirT, 10.1°C.
[h]WndSpd, 2.7 m/s; WtrT, 15.5°C; AirT, 9.9°C.
*There was light rain during this measurement.

using the maximum duration file length of 7.5 s for a data set of March 7, 2003, taken at a range of 1.62 km and where a Hanning window was applied prior to performing the FFT. In this and other PSD plots shown, high-frequency components in the plots are due to electrical or other noise and are not due to atmospheric fluctuations.

Note that, in general, the derived value of C_n^2 drops as the range increases. We believe that this is due to the geometry of the link. The test site is set back somewhat from the shore, thus the longer range slant paths pass higher above the ground than the shorter range paths. The scintillation close to the ground is higher, so the path-integrated C_n^2 values are higher as well.

Another useful diagnostic parameter of a laser communication channel is the probability of a fade, given a received signal level. The probability of a fade can be simply derived from the integrated PDFs. If we assume that the mean received power has a given margin above the required signal level for the detector, the PDF can be used to estimate the probability of a fade below the required level. Again, using the March 7 data, the fade probability is derived as a function of signal margin in decibels at 1.25, 1.6, and 2 km. The fade probability is plotted in Fig. 13 versus the signal level margin in decibels for these ranges.

Whereas the March 7 test was conducted on fairly calm water with the ambient air temperature slightly below and water temperatures just above 0°C, the April 15 test was characterized by choppy winds and relatively warm water and air temperatures of close to 10°C. The specific values are included in Table 2. The variability is exemplified by the variation in the second-by-second PDFs shown in Fig. 14. The individual profiles can be well fitted to the ΓΓ function, as demonstrated in Fig. 15, where the data taken in the 13th second is compared to the theoretical best fit curve, but an average of the PDFs taken for 1-s intervals over the whole 17-s interval fits less well. Later in the day when the turbulence became even higher, the PDF of the data taken at that time could not be fitted using the ΓΓ procedure, as can be seen in the example presented in Fig.

16. The PSD for one of the tests on April 15, 2003, is shown in Fig. 17.

The October 29, 2003, test was conducted under variable conditions with the water temperature being of the order of 15°C and the ambient air temperature about 10°C, but the winds diminished as the day progressed, ending with a period of light rain. The modulator array used was of a more compact design [Fig. 5(b)] and incorporated five modulators grown with a coupled-well design requiring only 5-V driving pulses. The 3-in. aperture interrogator was used and 25-s-duration data sets were stored of square-wave signals transmitted at between 1 and 5 Mbits/s, all five modulators receiving the same signal with the return basically coming from one MRR at any instance. The data presented in Figs. 18 and 19 correspond to the lowest level of turbulence encountered during all of these tests and occurred when light rain was falling at the end of the tests conducted on October 29, 2003. The PDFs on measured on a second-by-second basis were much more constant for the October data than for the April data and show a smaller range of intensity fluctuations. The PDF shown in Fig. 18 is the average of the PDFs for 1-s intervals taken over the 25-s data run and shows a reasonably good fit despite the very long data acquisition time.

8 Conclusions

This paper presented the first high-speed MRR link at ranges of a few kilometers. The same MRR array could support longer range links with an actively pointed interrogator using a narrower optical beam. Such a link would require no additional power on the modulator end.

The optimum design of a quantum-well MRR depends on many factors including contrast ratio, optical throughput, electrode structure, and retroreflector array design. The performance of a single MRR can be characterized by its modulation efficiency M, its drive voltage, its diameter, and its maximum bandwidth. Our current corner-cube-based devices have good performance at data rates of 10 Mbits/s or less. For higher data rates, cat's-eye devices are preferable.

Because quantum-well-based MRRs are capable of data rates of megabits per second, or higher, high-bandwidth data, such as video, can be transmitted using them. These links operate with very low power, size, and weight on the retroreflector end. The 3-Mbits/s digital video link required 200 mW of power to drive all five modulators. Using a simple angle-of-arrival sensor it would be possible to drive just a single modulator, dropping power even further. Note, however, that the video digitizer itself consumed several watts. An optimum use of the technology for this application will require trades of modulator bandwidth and data compression.

An MRR link, like all free-space optical links, is degraded by scintillation. For these maritime links, we have been in the low to moderate turbulence regime. Using a separate optical measurement system that has been in place for over a year, we have found that daytime C_n^2 values over the Chesapeake Bay are generally between 1 and 5 $\times 10^{-15}\,\mathrm{m}^{-2/3}$ for a path that averages 20 m above the water's surface.[8] In matching our data to various models for scintillation, we have found qualitative agreements in low to moderate turbulence. In higher turbulence, the models do not seem to match as well. Measurements of scintillation under a variety of conditions are useful in estimating fade probabilities for system design. A more extensive measurement of link conditions as a function of weather and air and water temperatures is underway at NRL and may help to predict performance of free-space optical links.

Acknowledgments

We acknowledge the support of the Office of Naval Research.

References

1. H. Hemati, "Optical systems for free-space laser communications," *Proc. SPIE* **5173**, 64–68 (2003).
2. C. C. Davis, I. I. Smolyaninov, and S. D. Milner, "Flexible optical wireless links and networks," *IEEE Commun. Mag.* **41**(3), 51–57 (2003).
3. S. Arnon, "Optimization of urban optical wireless communication systems," *IEEE Trans. Wireless Commun.* **2**(4), 626–629 (2003).
4. S. Arnon, "The effects of atmospheric turbulence and building sway on optical wireless communication systems," *Opt. Lett.* **28**(2), 129–131 (2003).
5. C. M. Swenson, C. A. Steed, I. A. DeLaRue, and R. Q. Fugate, "Low power FLC-based retromodulator communications system," *Proc. SPIE* **2290**, 296–310 (1997).
6. G. O. Olsen, H. W. Mocker, N. A. Demma, and J. B. Ross, "Coherent CO_2 laser communication system with modulable retroreflectors," *Appl. Opt.* **34**(12), 2033–2044 (1995).
7. J. P. Hansen and S. Madhu, "Angle scintillations in the laser return from a retroreflector," *Appl. Opt.* **11**(2), 233–238 (1972).
8. C. I. Moore, H. R. Burris, Jr., M. R. Suite, M. F. Stell, M. J. Vilcheck, M. A. Davis, R. Smith, R. Mahon, W. S. Rabinovich, J. P. Koplow, S. W. Moore, W. J. Scharpf, and A. E. Reed, "Free-space high-speed laser communication link across the Chesapeake Bay," *Proc. SPIE* **4821**, 474–485 (2002).
9. J. J. Degnan, "Millimeter accuracy satellite laser ranging: a review," in *Contributions of Space Geodesy to Geodynamics Technology*, D. E. Smith and D. L. Turcotte, Eds., AGU Geodynamics Series, Vol. 25, pp. 133–162, American Geophysial Union, Washington, DC (1993).
10. G. C. Gilbreath, W. S. Rabinovich, R. Mahon, D. S. Katzer, K. Ikossi-Anastasiou, M. R. Corson, J. F. Kline, J. H. Resnick, H. C. Merk, and M. J. Vilcheck, "Modulating retroreflector architecture using multiple quantum wells for free space optical communications," *Proc. SPIE* **3491**, 581–586 (1998).
11. W. S. Rabinovich, G. C. Gilbreath, P. G. Goetz, R. Mahon, D. S. Kazter, K. Ikossi-Anastasiou, S. Binari, T. J. Meehan, M. Ferraro, I. Sokolsky, J. A. Vasquez, and M. J. Vilcheck, "InGaAs multiple quantum well modulating retro-reflector for free space optical communications," *Proc. SPIE* **4489**, 190–201 (2001).
12. P. G. Goetz, R. Mahon, T. H. Stievater, W. S. Rabinovich, and S. C. Binari, "High-speed large area surface-normal multiple quantum well modulators," *Proc. SPIE* **5160**, 346–354 (2003).
13. M. L. Biermann, W. S. Rabinovich, R. Mahon, and G. C. Gilbreath, "Design and analysis of a diffraction-limited cat's-eye retroreflector," *Opt. Eng.* **41**(7), 1655–1660 (2002).
14. W. S. Rabinovich, P. G. Goetz, R. Mahon, E. Waluschka, D. S. Katzer, S. C. Binari, M. L. Biermann, and G. C. Gilbreath, "A cat's eye quantum well modulating retro-reflector," *IEEE Photonics Technol. Lett.* **15**(3), 401–403 (2003).
15. W. S. Rabinovich, P. G. Goetz, R. Mahon, L. Swingen, J. Murphy, G. C. Gilbreath, S. Binari, and E. Waluschka, "Performance of cat's eye modulating retro-reflectors for free-space optical communications," *Proc. SPIE* **5550**, 104–114 (2004).
16. G. C. Gilbreath, W. S. Rabinovich, T. J. Meehan, M. J. Vilcheck, R. Mahon, R. Burris, M. Ferraro, I. Solkolsky, J. A. Vasquez, C. S. Bovais, K. Cochrell, K. C. Goins, R. Barbehenn, D. S. Katzer, K. Ikossi-Anastasiou, and M. J. Montes, "Large-aperture multiple quantum well modulating retroreflector for free-space optical data transfer on unmanned aerial vehicles," *Opt. Eng.* **40**(7), 1348–1356 (2001).
17. D. A. B. Miller, D. S. Chelma, T. C. Damen, A. C. Gossard, W. Wiegmann, T. H. Wood, and C. A. Burrus, "Electric field dependence of optical absorption near the band gap of quantum well structures," *Phys. Rev. B* **32**(2), 1043–1060 (1985).
18. M. N. Islam, R. L. Hillman, D. A. B. Miller, and D. S. Chelma, "Electroabsorption in a GaAs/AlGaAs coupled quantum well waveguide," *Appl. Phys. Lett.* **50**(16), 1098–1100 (1987).
19. T. H. Stievater, W. S. Rabinovich, P. G. Goetz, R. Mahon, and S. C. Binari, "A surface-normal coupled-quantum-well modulator at 1.55 microns," *IEEE Photonics Technol. Lett.* **16**(9), 2036–2038 (2004).
20. B. J. Klein and J. J. Degnan, "Optical antenna gain. 1: Transmitting antennas," *Appl. Opt.* **13**(9), 2134–2140 (1974).
21. L. C. Andrews and R. L. Phillips, *Laser Beam Propagation through*

Random Media, SPIE Optical Engineering Press, Bellingham, WA (1998).
22. L. C. Andrews, R. L. Phillips, and C. Y. Hopen, *Laser Beam Propagation Scintillation with Applications*, SPIE Optical Engineering Press, Bellingham, WA (2001).
23. V. A. Banakh and V. L. Mironov, *LIDAR in a Turbulent Atmosphere*, Artech, Dedham, MA (1987).
24. L. C. Andrews, R. L. Phillips, and W. B. Miller, "Mutual coherence function for a double-passage retroreflected optical wave in atmospheric turbulence," *Appl. Opt.* **36**(3), 698–708 (1997).
25. J. H. Churnside and J. J. Wilson, "Enhanced backscatter of a reflected beam in atmospheric turbulence," *Appl. Opt.* **32**(15), 2651–2655 (1993).

Biographies and photographs of the authors not available.